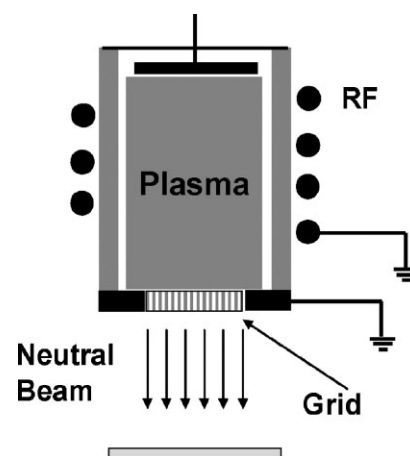


Modeling and Simulation of Fast Neutral Beam Sources for Materials Processing

Demetre J. Economou

Fast (kinetic energy of 10 to some 100 eV) neutral beams can be used for etching, deposition or surface modification, without charging damage that may occur in conventional plasma processing of materials. This paper provides an overview of the modeling and simulation approaches applicable to neutral beam sources. Neutral beam sources based on both volume and surface neutralization of ions are discussed, with emphasis on the latter.



Introduction

Low-temperature non-equilibrium plasmas have made and continue to make possible the incredible shrinking of integrated circuit feature dimensions. Plasma etching can replicate fine-line features into silicon and other materials with complete fidelity, due to anisotropic ion bombardment normal to the surface.^[1] The width of features in complimentary metal oxide semiconductor (CMOS) integrated circuits is currently as small as ≈ 40 nm, with some layers approaching one monolayer thickness. Plasma etching, deposition and surface modification will play a major role in both top-down (lithographic or stamped patterning) and bottom-up (e.g., self-assembled monolayer) nanotechnology at the sub-10-nm scale. However, plasma processes at nanoscale dimensions face several “road blocks,” notably plasma-induced charging damage.

Several forms of charging damage can be the result of differential charging of microfeatures during conventional plasma processing.^[2] Differential charging can deflect ions towards the feature sidewalls, inducing sidewall damage (bowing, notching, microtrenching) and reducing the ion flux at the bottom of the feature. The reduction of the ion flux as a function of depth in a feature can lead to aspect ratio dependent etching (ARDE), or even etch stop.^[3] This is a very complex process where, in addition to charging, imperfect collimation of the bombarding ions, depletion of reactants by sidewall reactions, polymer deposition, and redeposition of reaction products may also play a role.^[4]

Charging is expected to be more prevalent when etching polymers, oxide and other dielectrics. As device dimensions continue to shrink and feature aspect ratios keep increasing, charging problems will become even more severe. For example, profile twisting and distortion of the profile cross section^[5] have been observed in very high aspect ratio (>20:1) oxide etching. Charging of wafers exposed to a plasma can also lead to gate oxide breakdown.^[6]

Charging artifacts could be reduced or eliminated by using energetic neutral beams (fast atoms or molecules), instead of ions, to give the directional component of

D. J. Economou
Plasma Processing Laboratory, Department of Chemical and
Biomolecular Engineering, University of Houston, Houston TX
77204-4004, USA
E-mail: economou@uh.edu



Demetre J. Economou earned a Ph.D. in Chemical Engineering (1986) from the University of Illinois at Urbana-Champaign. Since 1986 he has been with the Chemical and Biomolecular Engineering Department at the University of Houston, where currently he is a *John and Rebecca Moores Professor* and the Associate Chairman of the Department. His research interests include plasma science and technology and nanotechnology.

reactive etching.^[7] For, while surfaces might still charge through secondary electron emission, there would be no effect on the neutral particle trajectories and, hence, no charging contribution to ARDE, sidewall bowing or notching. To be competitive with conventional reactive ion etching (RIE), neutral beams must have similar characteristics in terms of flux, energy, degree of collimation and large area coverage.

This paper provides an overview of modeling and simulation of interest to neutral beam sources, with emphasis on fast (kinetic energy of some 10 to some 100 eV) neutral beams for materials processing. Specific applications of neutral beams are summarized in refs.^[7,8]

Generation of Fast Neutral Beams

Fast neutral beams can be generated by neutralization of ion beams. There are two common methods to neutralize an ion beam: volume neutralization and surface neutralization. Ions extracted from a plasma source (for example gridded ion source) can be neutralized in a charge-exchange cell (volume neutralization) or by impingement on a neutralizer plate (surface neutralization). Kuwano and Shimokawa,^[9] as well as Ichiki and Hatakeyama^[10] produced fast neutral beams by neutralizing ions in

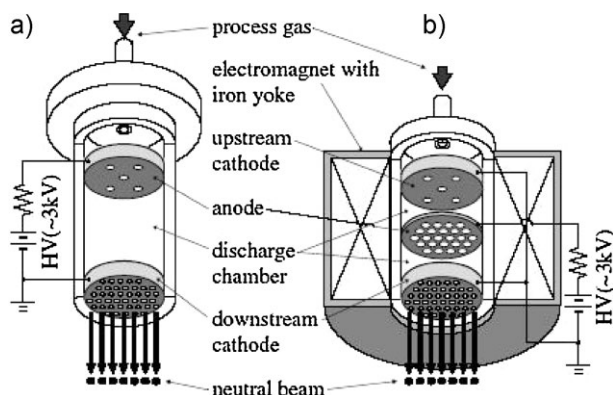


Figure 1. Neutral beam source based on volume neutralization of ions.^[10] A McIlraith DC cold-cathode discharge produces ions that are extracted through holes in the (lower) cathode plate. Ions are then neutralized by charge exchange with the gas downstream of the extraction electrode.

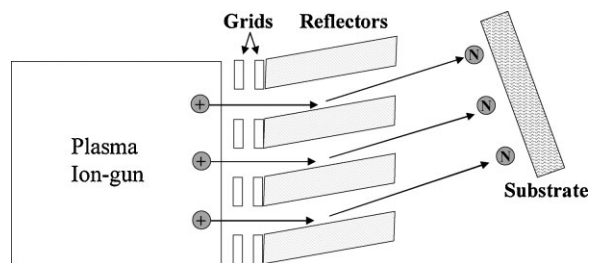


Figure 2. Neutral beam source based on surface neutralization of ions.^[13] Ions extracted from a gridded ion beam source are neutralized by grazing angle collisions on reflector plates.

charge exchange cells. Ions produced in McIlraith DC cold cathode discharges, were extracted through holes in a graphite cathode plate, and neutralized by charge exchange with the gas downstream of that plate (Figure 1). Goeckner et al.^[11] and Nichols and Manos^[12] produced neutral beams by reflecting accelerated ions off a metal surface at an angle with the ion beam. Kim et al.^[13] produced a fast neutral beam by extracting ions from a gridded ion source and neutralizing these ions by glancing angle collisions on the surfaces of a set of parallel metal plates (reflectors) next to the grids (Figure 2).

A more compact design uses the extraction grid itself as the ion neutralization surface. Simultaneous ion extraction and neutralization has the additional advantages of larger neutral beam flux and better control over beam characteristics. A neutral beam source based on simultaneous ion extraction and neutralization^[14] is shown in Figure 3. Ions generated in inductively coupled plasmas (ICP) are accelerated out of the plasma by a “beam acceleration electrode” in contact with the plasma. A boundary voltage (RF or DC) applied to the beam acceleration electrode controls the ion energy, and hence the resulting neutral beam energy (in the range of 20 to more than 200 eV). The boundary voltage raises the plasma potential, causing

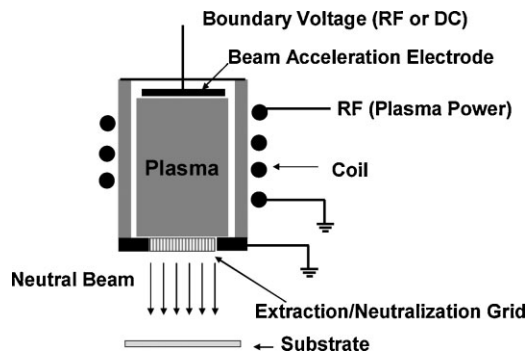


Figure 3. Neutral beam source based mainly on surface neutralization of ions.^[14] Ions extracted from a plasma through a grid with high aspect ratio holes are neutralized by grazing angle collisions on the internal surface of the holes of that grid.

positive ions to accelerate in the sheath over the grounded extraction/neutralization grid. While passing through the high aspect ratio grid holes, ions strike the internal surfaces of the holes (preferentially at grazing angles), and are converted to fast neutrals. Low pressure (<10 mTorr) in the plasma source (mean free path >1 cm) minimizes the probability of charge-exchange collisions between ions and slow neutrals, thus surface neutralization is dominant. The substrate is placed a small distance downstream of the extraction/neutralization grid in a differentially pumped processing chamber. The pressure in the processing chamber during operation of the source is typically more than 10× smaller than the pressure in the plasma (e.g., 10 mTorr in the plasma and 0.5 mTorr in the processing chamber). Low pressure minimizes gas phase scattering and helps beam collimation and flux.

Samukawa and co-workers^[15,16] also developed a fast neutral beam source based on simultaneous ion extraction and neutralization through a grid. A high density ICP was generated in a quartz tube. A bias was applied to an electrode in contact with the plasma (top electrode), to push ions through a parallel extraction electrode (bottom electrode). The extraction electrode had high aspect ratio through holes (1 mm diameter and 10 mm long). Ions suffered grazing angle collisions with the internal surfaces of the holes turning into fast neutrals. Charge exchange with neutral gas may have also played a role in ion neutralization at higher pressures. The authors studied neutral beams based on both positive and negative ion extraction and neutralization. For negative ions, they used a pulsed discharge in an electronegative gas (Cl₂ or SF₆). In the afterglow of a pulsed electronegative discharge, electrons attach to molecules generating negative ions. Provided the afterglow period is long enough, an ion-ion plasma forms^[17] and negative ions can be “pushed out” of the plasma by applying a negative bias to the top electrode. An optional DC or RF (e.g., 600 kHz) bias can also be applied to the bottom (extraction) electrode to provide additional control over the neutral beam energy.

Volume Neutralization of Ions

Volume neutralization is based on the charge exchange between an ion beam and a background gas. For example, for an argon ion beam in a background of argon atoms,



whereby a fast (beam) ion is converted to a fast (beam) neutral, and a slow neutral (of the background gas) is converted to a slow ion. Data on the cross section of this process (p. 77 of ref.^[1]) can be fit to $\sigma = 47.05(1.0 - 0.0557\ln\varepsilon_i)^2$, where σ is the charge exchange

cross section and ε_i is the fast-ion energy.^[18] In this expression, the cross section is in units of 10^{-16} cm², while the ion kinetic energy must be in eV.

Charge exchange reaction (1) does not alter the directionality of the fast ion. In addition, resonant charge exchange (between an ion and its parent neutral) has a cross section which is often an order of magnitude larger than the corresponding non-resonant charge exchange. The charge exchange cell pressure [or more precisely the product of background neutral density and cell length, NL , see Equation (4) below] should be high enough to achieve substantial neutralization but not too high to minimize beam scattering, that reduces the beam flux and directionality. Several researchers have reported on neutral beam sources based on volume neutralization of ions.^[10,19,20]

A simple analysis can be used to calculate the fraction of the ion beam that is neutralized by charge exchange collisions through a background gas. If I is the ion beam flux traveling through a gas of density N , the differential amount dI of beam neutralized over a distance dL is:

$$dI = -\sigma IN dL \quad (2)$$

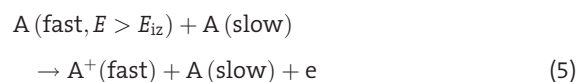
or

$$I = I_0 \exp(-\sigma N_{av}L) \quad (3)$$

The fraction of the beam neutralized will then be,

$$F_{\text{neutr}} = 1 - \frac{I}{I_0} = 1 - \exp(-\sigma N_{av}L) \quad (4)$$

where N_{av} is the average background gas density over length L . Actually, a fraction of the fast neutral beam may be re-ionized in fast atom-atom collisions of the sort,



where E is the energy of the fast atom and E_{iz} is the ionization potential. An ionization cross-section of $\approx 10^{-16}$ cm² has been experimentally measured for fast argon atoms with energy ≈ 100 eV colliding with thermal argon atoms.^[21] The ionization cross section is a strong function of the fast-atom energy.

Surface Neutralization of Ions

Ions coming in contact (within ≈ 1 Å) with a surface are, for example, Auger neutralized. The neutralization efficiency and properties (angle, energy) of the reflected neutral depend, among other variables, on the kind of impinging

ion, its energy and angle, and the kind, roughness and condition (e.g., adsorbed impurities) of the neutralizing surface. In general, negative ions tend to neutralize more efficiently compared to positive ions. In addition, negative ions can neutralize even on insulating surfaces,^[22] in contrast to positive ions that can eventually build up a potential equal to the ion energy. The angle of impact of ions on the surface is critical. Ions impacting the surface at grazing angles are more likely to scatter forward,^[23] and lose a small fraction of their impact energy. Thus, the emerging neutral beam retains more of the energy and directionality of the parent ion beam. In contrast, ions impacting nearly perpendicular to the surface, will scatter more diffusively, and will lose a larger fraction of their impact kinetic energy. The neutralization of ions by grazing collisions with a metal surface has been studied extensively.^[24] However, data on ion scattering off rough, practical surfaces, possibly “contaminated” by reaction byproducts, that are encountered in a neutral beam source, are lacking.

A way to predict the fate of an ion beam interacting with a surface is through molecular dynamics (MD) simulation.^[23] MD is a deterministic simulation of the motion of each and every atom in the simulation cell following the classical Newton's law. The force on an atom is computed based on the gradient of the interatomic potential function. Determination of this function (empirically or by *ab initio* methods) is critical for the success of the MD simulation. To execute the simulation, one starts with a cell (typically several 1 000 atoms) that simulates the system of interest (e.g., crystalline silicon). Ions, with given energy and angle, are then directed towards the surface of the cell, and are allowed to interact with the surface. Ions are assumed to neutralize just before impacting the surface, resulting in a neutral species interaction with the surface. The outcome of the interaction (reflection angle, reflection energy, etc.) is recorded. This procedure is repeated for some 100 to several 1 000 ion impacts to collect adequate statistics.^[23] Unfortunately, MD is not able to provide information on the effect of surface roughness (other than roughness on the atomic scale) on the ion scattering characteristics. A less computationally intensive method is to use the transport of ions in matter (TRIM) Monte Carlo code.^[25] One simulates a sufficiently large number of ion impacts at different angles and impact energies, and tabulates the output in terms of reflection coefficients, energy and angle distributions. In some cases, analytical expressions may be derived.^[26]

A simple model^[23] to calculate the energy of the reflected particles assumes specular scattering of the projectile off the surface, suffering two successive binary collisions with surface atoms. Then:

$$\sqrt{\frac{\varepsilon_r}{\varepsilon_i}} = \left(\frac{\mu}{\mu+1}\right)^2 \left(\cos \chi_{1/2} + \sqrt{\frac{1}{\mu^2} - \sin^2 \chi_{1/2}}\right)^2 \quad (6)$$

$$\chi_{1/2} = \frac{\pi}{2} - \theta_i, \quad \mu = \frac{m_i}{m_{\text{wall}}}$$

Here m_i and m_{wall} are the mass of the ion and the surface material atom, respectively. Also, θ_i is the angle of incidence, and ε_{in} and ε_r are kinetic energy of the incident and reflected species, respectively.

Neutral Beam Source Modeling and Simulation

Modeling and simulation of neutral beam sources can be broken down into constituent parts according to the components of the physical system:

1. Plasma reactor.
2. Ion beam transport.
3. Ion neutralization.
4. Neutral beam transport.
5. Neutral beam interaction with the substrate.

The division between plasma reactor and (ion or neutral) beam transport is clearer in the cases shown in Figure 1 and 2, since ion extraction through the grid and ion neutralization are rather well separated. In systems using simultaneous beam extraction and neutralization, however, this division is not as clear (Figure 3). Neutral beam interaction with the substrate will not be addressed here, because, even ions interacting with a substrate for the purpose of surface modification (etching, deposition, etc.) are modeled as neutrals.

Plasma reactor modeling and simulation has been the subject of intense studies over the past couple of decades. Because of the strong coupling between plasma physics and chemistry, and the vast range of spatial and time scales involved, plasma reactor simulation is still an extremely challenging task. One way to attack the problem is to break it down into smaller pieces, separating the length and time scales. For example, the plasma volume may be separated into bulk plasma and sheath. This is particularly convenient in high density plasma systems, in which the sheath is extremely thin (100 μm), while the reactor length scale is much larger (some 10 cm). In many cases, bulk plasma and sheath are solved together, i.e., the same equation set is applied to the whole reactor. This approach is especially prevalent for low density plasma systems, in which the sheath thickness is an appreciable fraction of the reactor length scale,^[27] but has also been practiced in high plasma density reactors.^[28] The reactor scale model is further split into “modules” (see Figure 4) to separate the disparate time scales of electron, ion, and neutral transport.^[29] This is essentially an equation splitting approach. Calculation of the electron energy distribution function (EEDF) by solving the Boltzmann equation is then part of the electron transport module. The EEDF determines the space- and time-dependent electron

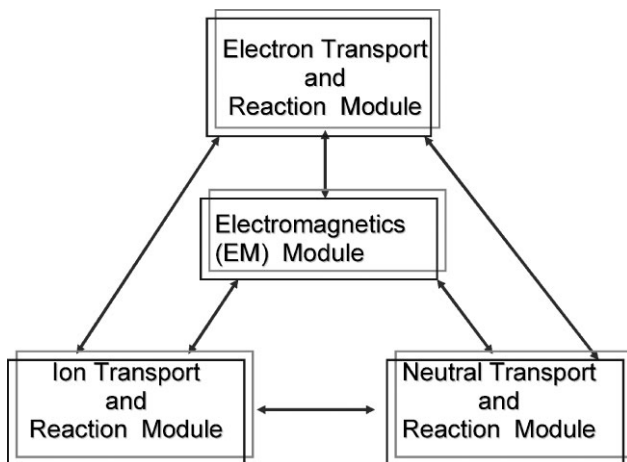


Figure 4. Time splitting approach in the simulation of plasma reactors. Electrons, ions and neutrals are each solved on their own time scale to speed up convergence of the simulation. The Maxwell equations (electromagnetics) are solved periodically to obtain the electric field. Information is cycled among the “modules” until a steady state is reached.^[29]

energy and transport properties, as well as the electron-particle (e.g., ionization) reaction rate coefficients.

Plasma reactor simulations range from zero-dimensional (well-mixed) to three-dimensional. Well mixed^[30] and one-dimensional models (including plug flow models^[31]), are best for sorting out the complicated gas and surface chemistry to arrive at a reduced reaction set for use in multidimensional simulations. Two-dimensional simulations can address the important aspect of reaction uniformity across the wafer radius.^[28] Three-dimensional simulations are useful for studying azimuthal asymmetries in the reactor due to non-axisymmetric power deposition, or non-axisymmetric gas inlets and pumping ports.^[32,33]

There are three kinds of glow discharge simulations: fluid, kinetic and hybrid. Fluid simulations use moments of the Boltzmann equation describing species density, momentum and energy conservation.^[34] They require some assumptions regarding the species distribution function (usually taken as Maxwellian) to achieve closure of the equations. Kinetic simulations, including particle-in-cell with Monte Carlo collisions (PIC-MCC),^[35] or direct simulation Monte Carlo (DSMC)^[36,37] yield the particle distribution functions as an output of the simulation. They are considered more accurate than fluid simulations at low pressures when the species mean free path λ is comparable to or longer than a characteristic length scale L (the Knudsen number, $Kn = \lambda/L > 0.1-1$), or for highly non-equilibrium situations. However, there is evidence that fluid simulations can perform well even at low pressures for which their assumptions must be scrutinized.^[38] Kinetic simulations are computationally intensive as compared to fluid simulations. Hybrid simulations

were developed^[39] in an attempt to preserve the accuracy of kinetic simulations and reduce the computational burden at the same time. A typical hybrid simulation treats the plasma species as interpenetrating fluids, but the EEDF is computed based on a Monte Carlo approach.^[40,41]

A fluid model consists of the coupled equations^[28] of mass continuity for electrons, ions and neutrals [Equation (7)], momentum continuity for the mixture [Equation (8)], energy continuity for neutrals [Equation (9)], and electrons [Equation (10)], and Poisson’s equation for the potential field [Equation (11)]. The ion temperature is often assumed equal to the gas temperature T_g due to the comparable masses of ions and neutrals and the collisionality of the plasma. The continuum approximation is valid when the mean free path $\lambda \ll L$.

$$\frac{\partial \rho_s}{\partial t} + \nabla \cdot (\rho_s \mathbf{u}) = -\nabla \cdot \mathbf{J}_s + \sum_r R_{sr} \quad (7)$$

$$\frac{\partial (\rho \mathbf{u})}{\partial t} + \nabla \cdot (\rho \mathbf{u} \mathbf{u}) = -\nabla \cdot p + \nabla \cdot \Pi + \rho \mathbf{g} \quad (8)$$

$$\begin{aligned} \frac{\partial (\rho_n e_n)}{\partial t} + \nabla \cdot (\rho_n e_n \mathbf{u}) = & -\nabla \cdot \sum_{\text{neutrals}} (\mathbf{q}_s + h_s \mathbf{J}_s) \\ & -p_n \nabla \cdot \mathbf{u} + \sum_{\text{neutrals}} \frac{\mathbf{J}_s}{\rho_s} \cdot \nabla p_s + \sum_{\text{neutrals}} Q_{es} \\ & + \sum_{\text{neutrals}} Q_{ce,s} + \sum_r \sum_{\text{neutrals}} R_{sr} H_{sr} \end{aligned} \quad (9)$$

$$\begin{aligned} \frac{\partial (\rho_e e_e)}{\partial t} + \nabla \cdot (\rho_e e_e \mathbf{u}) = & -\nabla \cdot (\mathbf{q}_e + h_e \mathbf{J}_e) - p_e \nabla \cdot \mathbf{u} \\ & + \frac{\mathbf{J}_e}{\rho_e} \cdot \nabla p_e - \mathbf{J}_e \cdot \mathbf{eE} - \sum_{s \neq e} Q_{es} + \sum_r R_{er} H_{er} \end{aligned} \quad (10)$$

$$\nabla^2 \Phi = -\frac{e}{\epsilon_0} \left(\sum_i z_i n_i - n_e \right) \quad (11)$$

In the above equations, subscript s denotes species including electrons ($s = e$), different kinds of ions ($s = i$), and different kinds of neutrals ($s = n$). Subscript r sums over all gas-phase chemical reactions. ρ_s is the species density (number density n_s times molecular mass m_s), ρ is the total density of the mixture, \mathbf{u} is the mass-average velocity of the mixture, and \mathbf{J}_s is the mass diffusion flux due to gradients in species density, pressure, and electric potential. R_{sr} denotes the mass rate of production or consumption of species s in reaction r . Π is the viscous stress tensor, \mathbf{g} is the acceleration of gravity, and p is the total pressure, which is the sum of all partial pressures (including electrons). $\rho_n e_n$ and $\rho_e e_e$ are the thermal energy of neutrals and electrons, respectively; \mathbf{q}_s and h_s are the

thermal conduction flux and specific enthalpy of species s , respectively; Q_{es} and $Q_{ce,s}$ are the energy exchange terms between electrons and species s (elastic collisions), and ions and species s (elastic and charge exchange collisions), respectively. The (multicomponent) mass diffusion flux \mathbf{J}_s can be expressed according to the formulation of Ramshaw and Chang.^[42] The last (summation) term in Equation (9) represents gas heating due to chemical reactions. The last term in Equation (10) represents electron energy loss (or gain in superelastic collisions) due to inelastic collisions. Boundary conditions typically include: given inlet gas composition and flow rate, wall temperature, and outlet pressure. On walls, the positive ion flux is often set equal to the drift flux, the negative ion flux is set equal to zero, and the (net) electron flux is determined by the electron thermal flux and secondary electron emission coefficient. The neutral species flux is set according to the respective neutral reaction probability. Despite the collisional nature of the plasma, the EEDF is often non-Maxwellian.^[43]

When the ion (and fast neutral) distribution functions are of interest, a kinetic simulation is necessary. Two approaches have been popular in this respect. Test-particle Monte Carlo (MC) and PIC-MCC. In the test-particle MC method, the spatial and temporal ionization and electric field profiles are first obtained by a fluid simulation. Using a Monte Carlo method, the trajectory of ions generated in the plasma according to the now known ionization profiles, is followed in the established E-field, allowing for gas-phase collisions, until the ion strikes a surface. Statistics of the quantities of interest (e.g., impact energy, angle etc.) are then collected. The term “test particle” implies that the motion of the ions under study does not influence the electric field.

PIC-MCC is more accurate but also more computationally demanding. This method solves the Boltzmann equation (12) with appropriate initial and boundary conditions. The dynamics of a plasma can be described by the Boltzmann equation in phase space (\mathbf{x}, \mathbf{v}) , where \mathbf{x} and \mathbf{v} are particle location and velocity, respectively,

$$\frac{\partial f}{\partial t} + \mathbf{v} \cdot \frac{\partial f}{\partial \mathbf{x}} + \frac{\mathbf{F}}{m} \cdot \frac{\partial f}{\partial \mathbf{v}} = \left(\frac{\partial f}{\partial t} \right)_{\text{coll}} \quad (12)$$

Here f is the particle distribution function. In PIC-MCC^[35] a mesh (grid) is overlaying the particles over the computational domain. Based on the particle positions, charges are assigned to each mesh point and current densities are assigned to the faces between the mesh points (weighting). Maxwell's equations are then solved to compute the electric field and magnetic induction on the grid. The Lorentz force $\mathbf{F} = q(\mathbf{E} + \mathbf{v} \times \mathbf{B})$ acting on a particle with charge q is obtained from the computed fields by interpolation based on the particle position (another weighting). Particles are then moved according to New-

ton's law (deterministically),

$$\frac{d\mathbf{x}}{dt} = \mathbf{v} \quad \text{and} \quad \frac{d\mathbf{v}}{dt} = \frac{\mathbf{F}}{m} \quad (13)$$

Particle collisions are handled stochastically in a Monte Carlo module in-between field adjusting time steps. The motion-collision cycle is repeated until a steady-state is reached and the statistics are adequate to calculate the particle distribution functions.

Determination of the residual ion and fast neutral flux, energy and angular distributions, emanating from a fast neutral beam source, requires a kinetic simulation. (Residual ions are the non-neutralized ions emanating from the source.) In the absence of gas-phase collisions, the ion beam simulation can be decoupled from the fast neutral beam simulation. In this case, a collisionless PIC simulation suffices to model ion beam transport and interaction with the grid. The trajectories of fast neutrals, generated by collision of ions on the walls of the grid are followed, perhaps all the way until they strike the substrate. In the presence of gas-phase collisions, however, the ion and neutral transport are coupled. Ions (or plasma flow in general) can still be followed by PIC-MCC. The best approach to handle neutral transport is by Direct Simulation Monte Carlo (DSMC).^[36,37,44] DSMC can follow both fast and thermalized neutrals yielding, among others, the pressure distribution along the length of the grid holes and in the region downstream of the holes. This affects ion and fast neutral beam transport thorough gas-phase collisions. Since ion and neutral flows are coupled, one would have to iterate between the ion and neutral simulation until convergence. Although DSMC simulations of (thermalized) neutral flow through microchannels have been reported,^[45] there seem to be no DSMC simulations of fast neutral beams generated in microchannels.

Plasma Molding

The properties (flux, energy, directionality) of neutral beams generated by simultaneous extraction and neutralization of ions through grid holes (Figure 3) depend critically on the interaction of the plasma with the holes (plasma molding). Plasma molding^[46] refers to the ability of the plasma-sheath interface to “contour” along the topography of surface features in contact with the plasma (Figure 5). In the case of plasma in contact with a grid, plasma molding depends primarily on the diameter of the grid hole, D , as compared to the plasma sheath thickness, L_{sh} . When $L_{sh} \gg D$ (Figure 5, left), the plasma-sheath interface (meniscus) is essentially planar as if the hole were not present (e.g., a solid wall). In this case, ions enter the hole with the ion energy distribution (IED) and ion angular distribution (IAD) they would have striking a

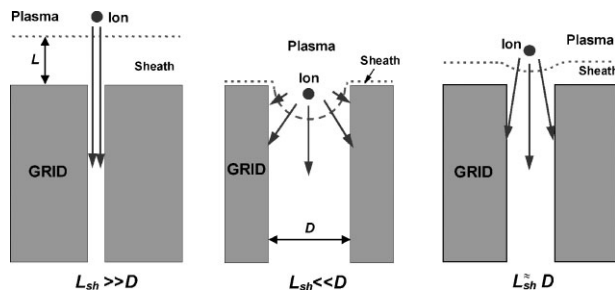


Figure 5. Plasma molding over surface topography. The sheath thickness L_{sh} is much larger (left), much smaller (middle) and comparable (right) to the hole diameter D .

planar wall (one dimensional sheath). These distributions have been studied extensively.^[47] For a low aspect ratio hole, most ions would exit the hole without colliding with the wall, i.e., as residual ions (assuming charge exchange collisions are negligible). The resulting ion flux and angular distribution at the hole exit can then be predicted based on geometric arguments alone. In this case, however, the fast neutral flux would be very small since most ions would preserve their charge in their transit through the hole.

In the other extreme, $L_{sh} \ll D$ (Figure 5, middle), the plasma “leaks” inside the hole. Plasma molding is severe, and the incoming ion trajectories are grossly perturbed. Most ions strike the sidewall and their impact angle is nearly perpendicular to the wall. These ions lose a large fraction of their impact energy during collision with the wall. The resulting neutral beam would have a large angular divergence and relatively low energy. In the intermediate case, $L_{sh} \approx D$ (Figure 5, right) the plasma-sheath meniscus “bends” gently over the hole. In this case, ions strike the sidewall at nearly grazing angles and lose a relatively small fraction of their energy upon collision.

When the sheath thickness is much larger than the diameter of the grid holes (Figure 5, left), the grid appears as a solid wall, and the plasma/sheath interface is planar (one-dimensional sheath). In this case, plasma reactor simulation is no different than the widely studied system of plasma over a substrate wafer.^[28,39,40] In the presence of plasma molding (Figure 5, center and right), however, the shape of the (multidimensional) plasma-sheath interface must be determined as part of the simulation. In general, the grid hole geometry necessitates a 3D simulation, a daunting task. For simplicity, the grid may be modeled as a set of concentric ring openings reducing the system dimensionality to 2D. On the other hand, the reactor may be simulated as a whole, or separated into bulk plasma and sheath. In the latter case, the bulk plasma simulation provides boundary conditions for the separate sheath simulation. For the multidimensional sheath simulation, a reasonable approximation is to focus on a single grid hole or a collection of several holes.^[48–50]

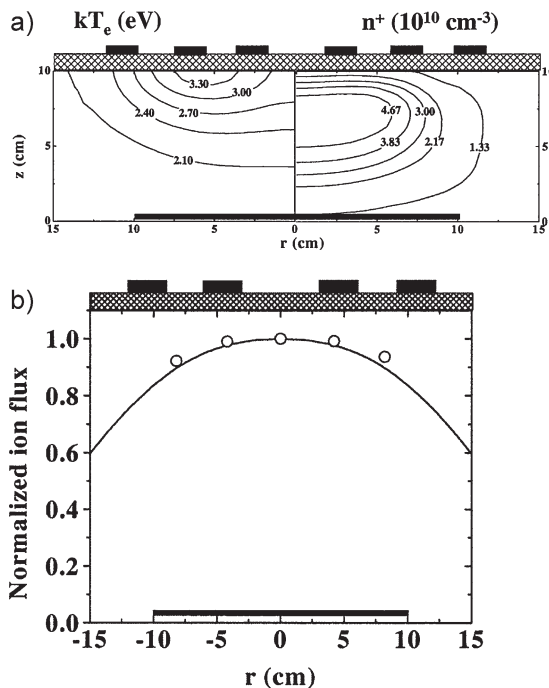


Figure 6. Electron temperature and positive ion density in a chlorine discharge^[51] sustained in an inductively coupled plasma reactor at 10 mTorr and 200 W (top). Positive ion flux profile across the substrate wafer (bottom). Line is simulation prediction and points are experimental data.

Results and Discussion

Figure 6 (top) shows the electron temperature and ion density distributions in a 10 mTorr, 200 W chlorine discharge sustained in an ICP reactor, predicted by a fluid simulation.^[51] The ion density profile yields an ion flux that peaks on axis. Should this reactor be used as a plasma source for an ion gun, the extracted ion flux would be maximum on axis, resulting in non-uniform etch or deposition rate. Kanarov et al.^[52] proposed a modification to the plasma source design to correct this problem. They used a re-entrant vessel design to suppress the ion flux maximum at the center of the reactor. They were able to achieve very high uniformity along a 300 mm wafer.

To illustrate plasma molding, Figure 7 displays electric potential profiles^[46] for a 500 μm -wide and 500 μm -deep 2D trench in contact with a high density plasma. Due to symmetry, only half of the trench is shown. The time-average sheath thickness L_{sh} was calculated on the wall far away from the trench (one-dimensional sheath). L_{sh} was smaller than, comparable to, and larger than the trench mouth width D for cases a), b), and c), respectively. Plasma molding along the surface topography of the trench is most severe for case a). In all cases, the sheath is locally thicker over the trench mouth and becomes thinner and planar away from the trench. As the ratio L_{sh}/D decreases [from c)–a)], the sheath becomes more conformal to the surface topography.

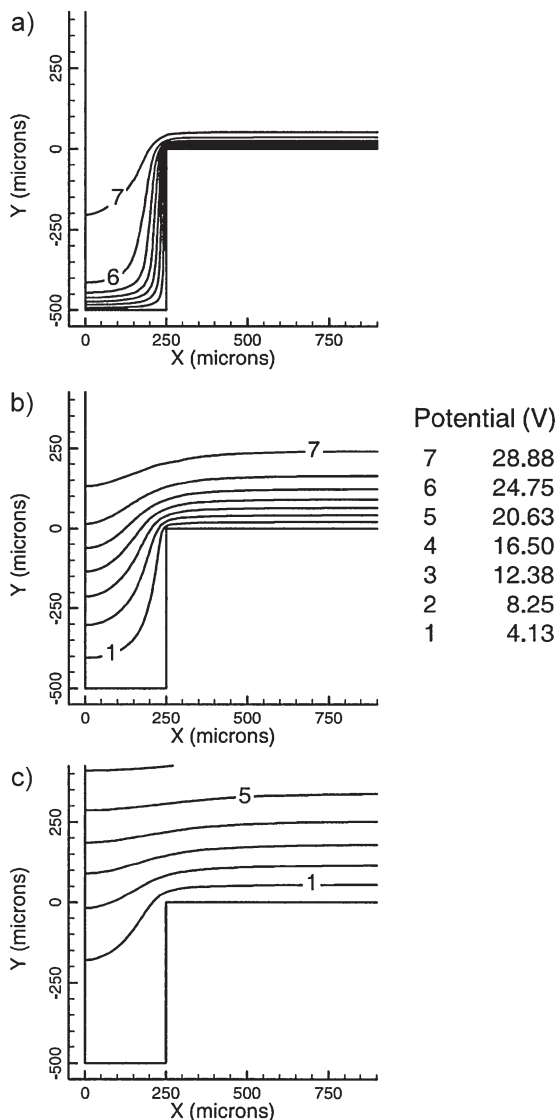


Figure 7. Electric potential contours around a 500 μm -wide and 500 μm -deep trench at $\tau_{rf} = 0$: a) $L_{sh} = 108 \mu\text{m}$ ($L_{sh}/D = 0.22$); b) $L_{sh} = 468 \mu\text{m}$ ($L_{sh}/D = 0.94$); c) $L_{sh} = 1281 \mu\text{m}$ ($L_{sh}/D = 2.6$). L_{sh} is the time-average sheath thickness calculated far away from the trench, where the sheath was one-dimensional.^[46]

Figure 8 shows the resulting electric field vector under the conditions of Figure 7. The electric field becomes significant within the sheath and keeps increasing as the wall is approached. The field strength outside the sheath is relatively negligible. Away from the trench, the electric field is vertical (one-dimensional) and the field strength depends on the sheath potential and thickness. Near the trench, the electric field becomes two-dimensional due to plasma molding, however. The maximum of the electric field is seen at the corner of the mouth of the trench. Because ions gain most of their kinetic energy in the sheath, the ion flux, IEDs, and IADs along the trench surface contour depend on the deformed electric field. For a

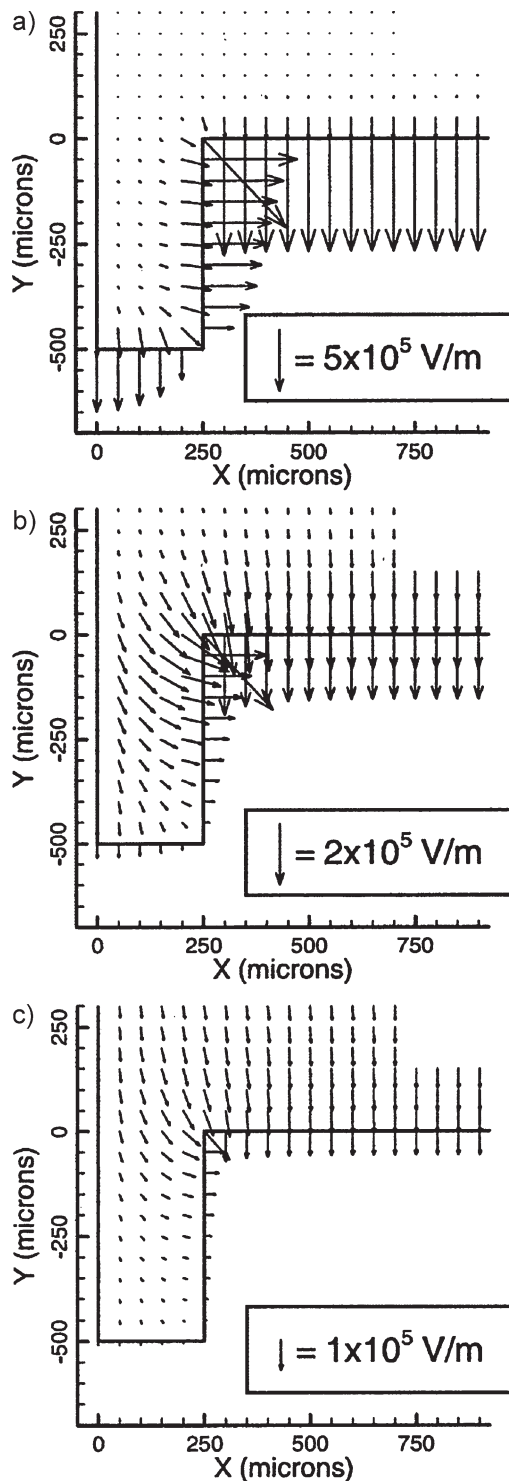


Figure 8. Electric field vector plots for the conditions of Figure 7: a) $L_{sh} = 108 \mu\text{m}$ ($L_{sh}/D = 0.22$); b) $L_{sh} = 468 \mu\text{m}$ ($L_{sh}/D = 0.94$); c) $L_{sh} = 1281 \mu\text{m}$ ($L_{sh}/D = 2.6$).^[46]

small sheath thickness (Figure 8a), $L_{sh}/D = 0.22$, the ion trajectories are drastically deformed inside the sheath, and a significant portion of ions strike the sidewall of the trench with small impact angles (almost perpendicular to

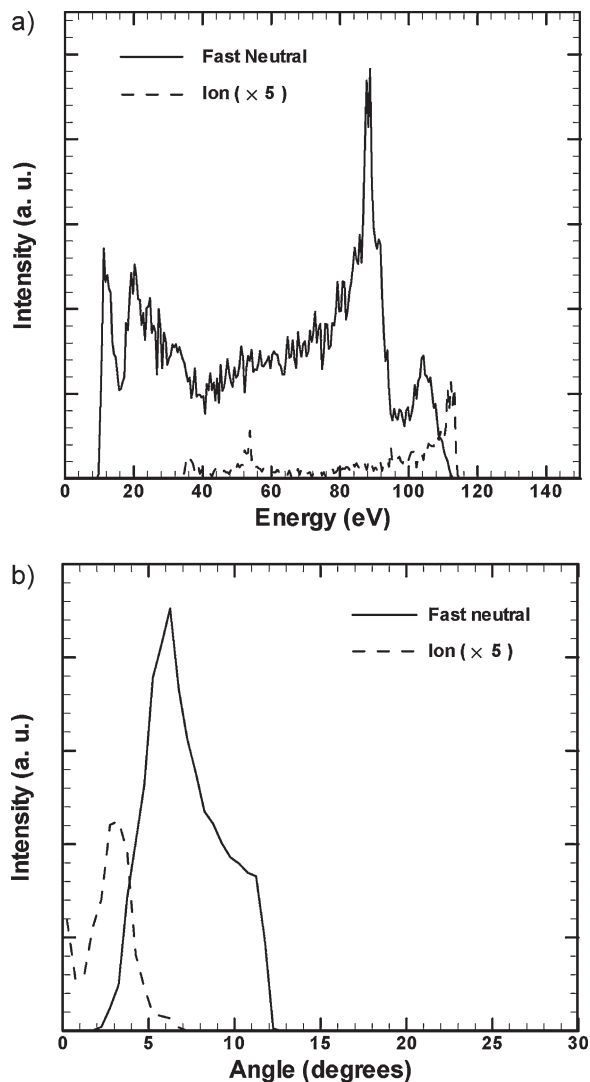


Figure 9. Residual ion and fast neutral energy distributions at the exit of a hole of a neutral beam source (top). Ion curve has been multiplied by 5 for clarity. Residual ion and fast neutral angular distributions at the hole exit (bottom). Ion curve has been multiplied by 5 for clarity. After ref.^[53]

the wall). When the sheath thickness is larger than the width of the trench (Figure 8c), $L_{sh}/D = 2.6$, plasma molding is weaker and a smaller portion of the sheath is deformed by the presence of surface topography. In this case, ions spend a significant amount of their sheath transit time in a region of vertical electric field. Due to their vertical momentum, ions are not affected as strongly by the horizontal electric field near and inside the trench. Consequently, ions strike the sidewall at grazing angles.

Figure 9 (top) shows the residual ion and fast neutral energy distributions downstream of the hole predicted by a PIC simulation.^[53] The hole was 0.154 mm in diameter and 1.078 mm in length (aspect ratio 7:1). The neutral energy distribution (NED) is shifted to lower energies compared to

the ion energy distribution (IED) due to energy loss by collision with the wall. [The energy loss was computed using Equation (6).] The simulation revealed that higher energy ions have larger (more grazing) angle of incidence; this results in less energy shift in the high energy region. Smaller energy ions generally collide at smaller angles and lose more energy, explaining the increased energy shift in the low energy region. Figure 9 (bottom) shows the ion and fast neutral angular distributions (NAD) downstream of the hole. The ion angular distribution (IAD) can't exceed about 8 degrees, the acceptance angle of the hole. The NAD is "empty" at small angles (donut shaped) because fast neutrals are generated only by reflection of ions striking the wall. Vertical or nearly vertical (with respect to the macroscopic grid surface) ions do not strike the wall and can't generate fast neutrals (Figure 5, left).

It appears that there is an optimum "bending" of the plasma-sheath meniscus over a hole that results in best neutral beam source performance. If the plasma-sheath meniscus is planar (thick sheath, Figure 5, left), ions entering the hole are highly directional and pass through the hole without collision with the sidewall. Thus, the neutralization efficiency is low, resulting in low neutral beam flux. On the other hand, if the plasma-sheath meniscus dips deep inside the hole (Figure 5, middle) almost all ions strike the sidewall and neutralize, resulting in higher neutral flux, but worse neutral beam directionality. In this case, since ions strike the sidewall at small angles (with respect to the normal on the sidewall), ions lose a larger fraction of their energy, reducing the energy of the fast neutral beam. Under these conditions, fast neutrals may also suffer multiple collisions with the sidewall worsening the situation. Nam et al.^[53] found that "optimum" neutral beams are extracted by maximizing the number of "good" ions entering the grid holes. In general, ions that neutralized on the top section of the hole sidewalls were "bad," in the sense that these ions yielded divergent neutral beams of relatively low energy. Ions that neutralized along the bottom (downstream) section of the hole sidewalls were "good," in the sense that these ions yielded neutral beams that were less divergent and retained more of the energy of the parent ions.

Kim et al.^[13,50,54] used a PIC simulation to compute the characteristics of a neutral beam source. Their system is shown schematically in Figure 2. The simulation was divided into two parts: ion gun and reflector plates. The ion gun had a dual grid (grid thickness 1.2 mm, grid spacing 0.9 mm, hole diameter 4 mm) and the potentials on the grids were set to achieve an ion energy of 300 V. The reflector plates were at an angle of 5° with respect to the ion gun axis. The argon pressure in the ICP source of the ion gun was 0.1 mTorr. Figure 10 (top) shows a snapshot of the ion distribution through the grids of the ion gun, while Figure 10 (bottom) shows the resulting fast neutrals

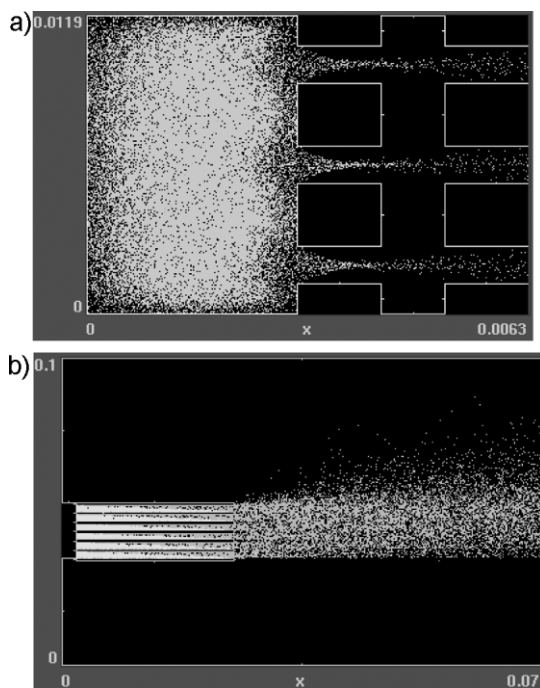


Figure 10. A snapshot of a particle-in-cell simulation of a neutral beam source of the kind shown in Figure 2. Ion distribution in the near grid region of the ion source (top). Ion (white) and fast neutral (green) distributions through and downstream of the reflector plates (bottom), after ref.^[50]

through the reflector plates. The energy and angle distributions on the substrate are shown in Figure 11. The average energy of the fast neutrals corresponds to $\approx 70\%$ of the parent ion energy. A significant fraction of the neutrals has low energies. These neutrals originate from ions that impact the surface at smaller angles (with respect to the surface normal) and/or neutrals suffering multiple collisions with the reflector plates. The angular distribution of the fast neutrals peaks several degrees off axis. These neutrals can be made nearly perpendicular to the substrate by tilting the substrate at the appropriate angle. The flux of fast neutrals at the substrate was only a few percent of the ion flux produced by the gun. Apparently, a large fraction of the ions was captured by the grids of the ion gun or thermalized completely in their transit through the reflector plates. The authors proposed a three-grid extraction system to achieve independent control of ion (hence fast neutral) flux and energy. Detailed studies of the effect of reflector plate geometry (size, separation, angle) are yet to be reported.

Neutral Beams with Small Energy Spread

Precise control of the energy distribution of energetic species (ions or fast neutrals) is becoming progressively more important as films require etching with monolayer accuracy.^[55] A neutral beam with a relatively tight energy

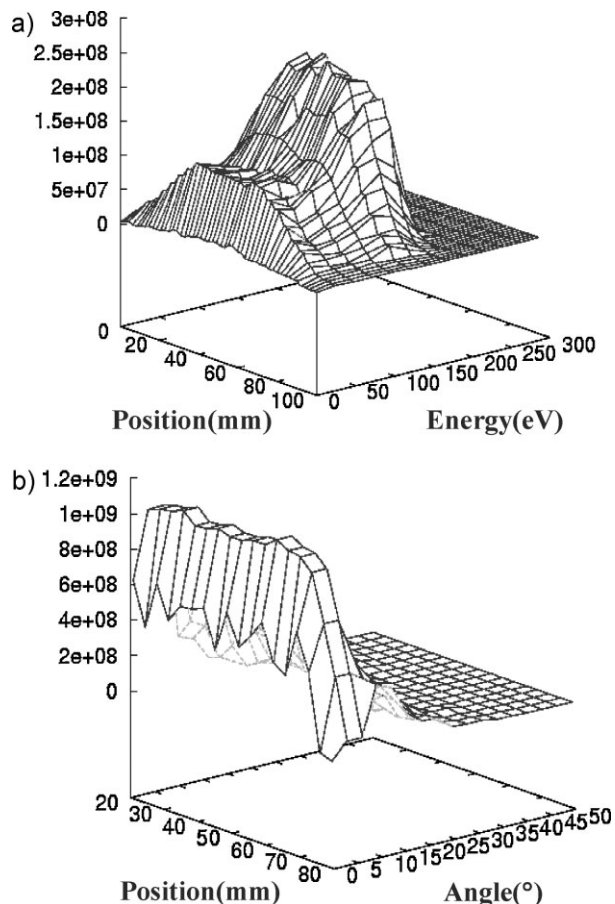


Figure 11. Fast neutral energy distribution (top) and fast neutral angular distribution (bottom) on the substrate calculated by the PIC simulation of the source shown in Figure 10, taken from ref.^[13]

spread may be produced by neutralization of a nearly monoenergetic ion beam. This may be accomplished with the system shown in Figure 3. The strategy used to obtain a nearly monoenergetic ion beam was described in refs.^[55,56] The RF plasma power was pulsed ON (active glow) and OFF (afterglow) with a certain frequency and duty ratio. A positive DC voltage was applied during a predetermined time window in the afterglow (synchronous boundary voltage) to the beam acceleration electrode (Figure 3). During the afterglow, the electric fields disintegrate and the electron temperature plummets within several μs . This results in a nearly uniform plasma potential of low value. Upon application of the boundary voltage, the plasma potential is raised to just above the value of that voltage, forcing positive ions out of the plasma, through the grounded extraction/neutralization grid. The ion energy is therefore set by the boundary voltage. Also, since the ion temperature (T_i) is a measure of random motion of ions, T_i affects the divergence of the ion beam. Because T_i scales with T_e , smaller T_e reduces the angular spread of the ion beam extracted in the afterglow.

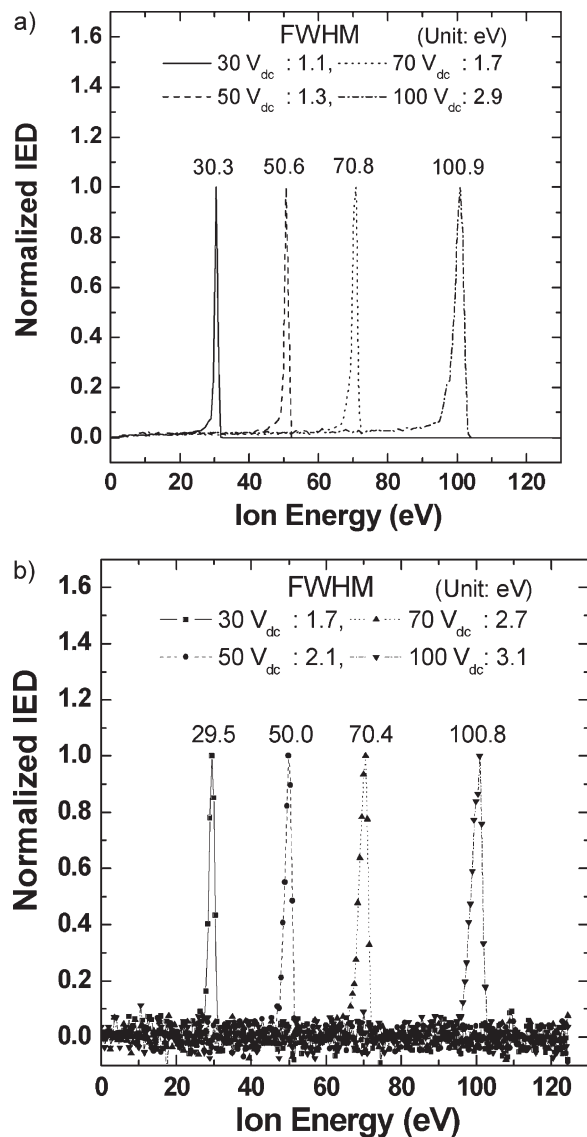


Figure 12. Nearly monoenergetic distribution of extracted ions for different DC bias potentials (30, 50, 70, and 100 V) applied in the afterglow (RF power off, top).^[48] Experimental data from ref.^[56] for the same conditions as in the simulation (bottom, FWHM = full width at half maximum).

A PIC simulation^[48] was used to predict the (residual) IED emanating from this source (Figure 12, top). Indeed, a nearly monoenergetic ion beam is obtained with energy controlled by the applied DC bias. The width of the IED increases from 1.1 eV at 30 V DC bias to 2.9 eV at 100 V DC bias. This is due to slight gradients in the plasma potential. The small tail on the left of the IEDs is due to infrequent charge exchange collisions of ions with neutrals. The corresponding experimental data^[56] are shown in Figure 12 (bottom). Very good agreement with the simulation results is obtained, except that the width of the experimental IEDs is a bit larger than predicted,

probably due to the finite resolution of the gridded ion energy analyzer used for measurements.

The PIC simulation predicted that plasma molding was minimal in this case since the sheath thickness was much larger than the grid hole diameter. Hence ions were accelerated by a one-dimensional (vertical) field through most of the sheath. Ions saw a horizontal component of the field near the hole entrance, but the vertical ion momentum was too high to divert ions from their path. Hence, the angular distribution of extracted ions was very narrow. In fact, as the applied DC bias voltage was increased, the angular spread decreased as the vertical velocity component of ions became greater. The half width at half maximum of the ion angular distribution was only 0.25° at 100 V applied DC bias in the afterglow.

Experimental data^[57] showed that the fast NED produced by neutralization of a nearly monoenergetic ion beam had a tighter full width at half maximum (FWHM = 14 eV) when compared to the fast NED produced by neutralization of ions extracted from a continuous wave plasma, under otherwise similar conditions (FWHM = 40 eV).

Conclusion

Directional, fast (kinetic energy some 10 to several 100 eV) neutral beams can mitigate charging damage that can occur during conventional plasma processing, especially for high aspect ratio nanoscale etching of insulating materials. Although ion beam sources with large area (300 mm diameter) uniform coverage have been demonstrated, large diameter neutral beam sources are yet to be developed. Modeling and simulation can be an invaluable tool for the design and optimization of these sources. Neutral beam source modeling and simulation faces many of the same issues encountered in conventional plasma reactors. These include large area uniformity and high flux of directional reactive species to the substrate. In addition, neutral beam sources must deal with the issue of ion extraction and neutralization through a grid or downstream of a grid. Modeling of neutral beam sources based on separate ion extraction and neutralization can benefit from the literature on ion beam sources.^[58] Kinetic simulations (PIC-MCC and DSMC) are best suited to ultimately predict the energy and angular distributions of fast neutrals impinging on the substrate. The physics of ion scattering off practical (possibly rough and “contaminated”) surfaces will continue to be of main interest in this respect. Simulations of product distribution in the etching chamber have not yet been reported. Significant pressure gradients may exist depending on geometry.^[59]

Acknowledgements: This work was supported by the *State of Texas* and *Tokyo Electron Limited*. Fruitful discussions with Drs. *Vince Donnelly* of the University of Houston and *Lee Chen* of Tokyo Electron are gratefully acknowledged. Many thanks to Dr. *J. Zhao* also of Tokyo Electron for bringing ref.^[22] to my attention.

Received: January 22, 2009; Revised: March 14, 2009; Accepted: March 16, 2009; DOI: 10.1002/ppap.200900005

Keywords: etching; modeling; neutral beams; PIC; plasmas

- [1] M. A. Lieberman, A. J. Lichtenberg, "Principles of Plasma Discharges and Materials Processing," 2nd Edition, Wiley, New York 2005.
- [2] J. C. Arnold, H. H. Sawin, *J. Appl. Phys.* **1991**, *70*, 5314.
- [3] J. Matsui, N. Nakano, Z. Lj., Petrovic, T. Makabe, *Appl. Phys. Lett.* **2001**, *78*, 883.
- [4] R. A. Gottscho, C. W. Jurgensen, D. J. Vitkavage, *J. Vac. Sci. Technol. B* **1992**, *10*, 2133.
- [5] S.-C. Park, S.-H. Lim, C.-H. Shin, G.-J. Min, C.-J. Kang, H.-K. Cho, J.-T. Moon, *Thin Solid Films* **2007**, *515*, 4923.
- [6] C. T. Gabriel, J. P. McVittie, *Solid State Technol.* **1992**, *35*, 81.
- [7] D. J. Economou, *J. Phys. D: Appl. Phys.* **2008**, *41*, 024001.
- [8] S. Samukawa, *Jpn. J. Appl. Phys., Part 1* **2006**, *45*, 2395.
- [9] H. Kuwano, F. Shimokawa, *J. Vac. Sci. Technol. B* **1988**, *6*, 1565.
- [10] K. Ichiki, M. Hatakeyama, *J. Phys. D: Appl. Phys.* **2008**, *41*, 024003.
- [11] M. J. Goeckner, T. K. Bennett, S. A. Cohen, *Appl. Phys. Lett.* **1997**, *71*, 980.
- [12] C. A. Nichols, D. M. Manos, *J. Appl. Phys.* **1996**, *80*, 2643.
- [13] S. J. Kim, S. J. Wang, J. K. Lee, D. H. Lee, G. Y. Yeom, *J. Vac. Sci. Technol. A* **2004**, *22*, 1948.
- [14] S. Panda, D. J. Economou, L. Chen, *J. Vac. Sci. Technol. A* **2001**, *19*, 398.
- [15] S. Samukawa, K. Sakamoto, K. Ichiki, *Jpn. J. Appl. Phys., Part 2* **2001**, *40*, L779.
- [16] S. Samukawa, K. Sakamoto, K. Ichiki, *J. Vac. Sci. Technol. A* **2002**, *20*, 1566.
- [17] D. J. Economou, *Appl. Surf. Sci.* **2007**, *253*, 6672.
- [18] D. Kim, D. J. Economou, *IEEE Trans. Plasma Sci.* **2002**, *30*, 2048.
- [19] K. Yokogawa, T. Yunigami, T. Mizutani, *Jpn. J. Appl. Phys.* **1996**, *35*, 1901.
- [20] Y. Jin, T. Tsuchizawa, S. Matsuo, *Jpn. J. Appl. Phys.* **1995**, *34*, L465.
- [21] P. O. Haugsjaa, R. C. Amme, *J. Chem. Phys.* **1970**, *52*, 4874.
- [22] J. Ishikawa, *Rev. Sci. Instrum.* **1998**, *69*, 863.
- [23] B. A. Helmer, D. B. Graves, *J. Vac. Sci. Technol. A* **1998**, *16*, 3502.
- [24] [24a] J. W. Rabalais, J.-N. Chen, R. Kumar, N. Narayana, *J. Chem. Phys.* **1985**, *83*, 6489; [24b] H. Kang, S. R. Kasi, J. W. Rabalais, *J. Chem. Phys.* **1988**, *88*, 5882; [24c] H. Kang, S. R. Kasi, O. Grizzi, J. W. Rabalais, *J. Chem. Phys.* **1988**, *88*, 5894; [24d] S. R. Kasi, M. A. Kilburn, H. Kang, J. W. Rabalais, L. Tavernini, P. Hochmann, *J. Chem. Phys.* **1988**, *88*, 5902; [24e] S. R. Kasi, H. Kang, J. W. Rabalais, *J. Chem. Phys.* **1988**, *88*, 5914.
- [25] [25a] J. F. Ziegler, J. P. Biersack, U. Littmark, "The Stopping and Range of Ions in Solids", Pergamon Press, New York 1985; [25b] W. Eckstein, J. P. Biersack, *Appl. Phys. A* **1985**, *A38*, 123.
- [26] Y. Tokunaga, Y. Kurita, M. Sugihara, S. Hitoki, S. Saito, *Comput. Phys. Commun.* **1985**, *38*, 15.
- [27] D. P. Lymberopoulos, D. J. Economou, *J. Vac. Sci. Technol. A* **1994**, *12*, 1229.
- [28] D. Bose, T. R. Govinda, M. Meyyappan, *J. Electrochem. Soc.* **1999**, *146*, 2705.
- [29] D. J. Economou, *Thin Solid Films* **2000**, *365*, 348.
- [30] E. Meeks, J. W. Shon, *IEEE Trans. Plasma Sci.* **1995**, *23*, 539.
- [31] L. E. Kline, W. D. Partlow, W. E. Bies, *J. Appl. Phys.* **1989**, *65*, 70.
- [32] M. J. Kushner, *J. Appl. Phys.* **1997**, *82*, 5312.
- [33] T. Panagopoulos, V. Midha, D. Kim, D. J. Economou, *J. Appl. Phys.* **2002**, *91*, 2687.
- [34] *Computational Modeling in Semiconductor Processing*, M. Meyyappan, Ed., Artech House, Boston 1994.
- [35] C. K. Birdsall, *IEEE Trans. Plasma Sci.* **1991**, *19*, 65.
- [36] G. A. Bird, "Molecular Gas Dynamics and the Direct Simulation of Gas Flows", Oxford University Press, Oxford 1994.
- [37] D. J. Economou, T. J. Bartel, R. S. Wise, D. P. Lymberopoulos, *IEEE Trans. Plasma Sci.* **1995**, *23*, 581.
- [38] M. Surendra, *Plasma Sources Sci. Technol.* **1995**, *4*, 56.
- [39] P. L. G. Ventzek, R. J. Hoekstra, M. J. Kushner, *J. Vac. Sci. Technol. B* **1994**, *12*, 461.
- [40] A. Sankaran, M. J. Kushner, *J. Vac. Sci. Technol. A* **2004**, *22*, 1242.
- [41] S. Tinck, W. Boullart, A. Bogaerts, *J. Phys. D: Appl. Phys.* **2008**, *41*, 065207.
- [42] J. D. Ramshaw, C. H. Chang, *Phys. Rev. E* **1996**, *53*, 6382.
- [43] V. A. Godyak, R. B. Piejak, B. M. Alexandrovich, *Plasma Sources Sci. Technol.* **1992**, *1*, 36.
- [44] V. Serikov, K. Nanbu, *J. Vac. Sci. Technol. A* **1996**, *14*, 3108.
- [45] R. E. Chamberlin, N. A. Gatsonis, *Nanoscale Microscale Thermophys. Eng.* **2008**, *12*, 170.
- [46] D. Kim, D. J. Economou, J. R. Woodworth, P. A. Miller, R. J. Shul, I. C. Abraham, B. P. Aragon, T. W. Hamilton, *IEEE Trans. Plasma Sci.* **2003**, *31*, 691.
- [47] E. A. Edelberg, A. Perry, N. Benjamin, E. S. Aydil, *J. Vac. Sci. Technol. A* **1999**, *17*, 506.
- [48] S. K. Nam, D. J. Economou, V. M. Donnelly, *Plasma Sources Sci. Technol.* **2007**, *16*, 90.
- [49] S. K. Nam, D. J. Economou, V. M. Donnelly, *J. Phys. D: Appl. Phys.* **2006**, *39*, 3994.
- [50] M. S. Hur, S. J. Kim, H. S. Lee, J. K. Lee, G.-Y. Yeom, *IEEE Trans. Plasma Sci.* **2002**, *30*, 110.
- [51] T. W. Kim, E. S. Aydil, *IEEE Trans. Plasma Sci.* **2003**, *31*, 614.
- [52] V. Kanarov, A. Hayes, R. Yevtukhov, I. Kemeyama, D. Siegfried, E. Wahlin, *Rev. Sci. Instrum.* **2006**, *77*, 03B515.
- [53] S. K. Nam, D. J. Economou, V. M. Donnelly, *IEEE Trans. Plasma Sci.* **2007**, *35*, 1370.
- [54] S. J. Kim, H. J. Lee, G. Y. Yeom, J. K. Lee, *Jpn. J. Appl. Phys.* **2004**, *43*, 7261.
- [55] A. Agarwal, M. J. Kushner, *J. Vac. Sci. Technol. A* **2009**, *27*, 37.
- [56] L. Xu, D. J. Economou, V. M. Donnelly, P. Ruchhoeft, *Appl. Phys. Lett.* **2005**, *87*, 041502.
- [57] [57a] A. Ranjan, V. M. Donnelly, D. J. Economou, unpublished; [57b] A. Ranjan, *Ph.D. Thesis*, University of Houston 2008.
- [58] M. Irzyk, C. Laure, A. Bouchoule, *Plasma Sources Sci. Technol.* **2001**, *10*, 463.
- [59] D. J. Economou, T. J. Bartel, *IEEE Trans. Plasma Sci.* **1996**, *24*, 131.